PHYSICS OF FLUIDS VOLUME 10, NUMBER 9 SEPTEMBER

On the alignment of strain, vorticity and scalar gradient in turbulent, buoyant, nonpremixed flames

O. N. Boratav, S. E. Elghobashi, and R. Zhong
Mechanical and Aerospace Engineering Department, University of California, Irvine, California 92717

(Received 18 February 1998; accepted 20 May 1998)

The alignment of vorticity and scalar gradient with the eigendirections of the rate of strain tensor is investigated in turbulent buoyant nonpremixed horizontal and vertical flames. The uniqueness of a buoyant nonpremixed flame is that it contains regions with distinct alignment characteristics. The strain-enstrophy angle Ψ is used to identify these regions. Examination of the vorticity field and the vorticity production in these different regions indicates that Ψ and consequently the alignment properties near the flame surface identified by the mixture fraction band $F \approx F_{st}$ differ from those in the fuel region, $F > F_{st}$ and the oxidizer region, $F < F_{st}$. The $F \approx F_{st}$ band shows strain-dominance resulting in vorticity/α alignment while $F > F_{st}$ (and $F < F_{st}$ for the vertical flame) band(s) show(s) vorticity/β alignment. The implication of this result is that the scalar dissipation, ϵ_F, attains its maximum value always near $F \approx F_{st}$. These results are also discussed within the framework of recent dynamical results [Galanti *et al.*, Nonlinearity **10**, 1675 (1997)] suggesting that the Navier-Stokes equations evolve towards an attracting solution. It is shown that the properties of such an attracting solution are also consistent with our results of buoyant turbulent nonpremixed flames. © *1998 American Institute of Physics.* [S1070-6631(98)01709-7]

I. INTRODUCTION

More than 40 years ago, Batchelor and Townsend[1] suggested that the material lines consisting of fluid particles tend to align along the direction of the largest principal rate of strain, denoted by α. They also indicated[1] that this alignment is unlikely to be perfect since the principal axes of strain rotate relative to the fluid. Indeed, Kerr,[2] and Ashurst *et al.*,[3] observed that in homogeneous isotropic and homogeneous shear turbulence, the vorticity alignment is not with the largest strain direction but with the intermediate strain, denoted by β. Dresselhaus and Tabor[4] showed analytically that the competition between the strain and rotation determines whether the material (or vorticity) lines will align with α or β direction. Nomura and Elghobashi,[5] and Boratav *et al.*[6] showed that for the variable density flows of nonpremixed flames with heat release, the vorticity tends to align along the α strain direction.

The analyses of Dresselhaus and Tabor[4] and Boratav *et al.*[6] led to a vector equation which can be written for the most general case as:

$$\frac{d}{dt}\hat{\Lambda} = \begin{pmatrix} \alpha - D & 0 & 0 \\ 0 & \beta - D & 0 \\ 0 & 0 & \gamma - D \end{pmatrix} \hat{\Lambda} - \zeta \hat{\Lambda} - (\Omega' + \mathbf{C} - \Omega) \times \hat{\Lambda}. \quad (1)$$

The components of the unit vector $\hat{\Lambda}$ are the direction cosines of the unit material or vorticity element with respect to the strain orthonormal eigendirections $\hat{\mathbf{e}}_\alpha$, $\hat{\mathbf{e}}_\beta$ and $\hat{\mathbf{e}}_\gamma$, where α, β, γ denote the eigenvalues of the rate of strain tensor with the conventional ordering, $\alpha > \beta > \gamma$. The direction of the unit vector $\hat{\Lambda}$ is along the material or vorticity element. Ω' is the rotational velocity vector of the strain basis axes. $\mathbf{C}$ accounts for the coriolis effect of the baroclinic torque. For incompressible flows, the velocity divergence D, $(D = \alpha + \beta + \gamma)$, and the baroclinic term $\mathbf{C}$ are zero. For the vorticity element analysis, the cross product $\Omega \times \hat{\Lambda}$ is zero.

Dresselhaus and Tabor[4] examined the material element alignment for an incompressible flow and used the notation $\hat{\lambda}$ for $\hat{\Lambda}$. Boratav *et al.*[6] examined the vorticity element alignment and used the notation $\hat{\Omega}$ for the variable $\hat{\Lambda}$. ζ in Eq. (1) is a quadratic nonlinear term which contains the eigenvalues α, β and γ. In an incompressible flow, ζ is defined as $\zeta \equiv \zeta_{line} = \alpha\lambda_1^2 + \beta\lambda_2^2 + \gamma\lambda_3^2$. For the variable density vorticity alignment, our previous result[6] and further analysis show that $\zeta \equiv \zeta_{vorticity} = \alpha\Omega_1^2 + \beta\Omega_2^2 + \gamma\Omega_3^2 - D$. It can be shown that D appearing in the ζ definition cancels with that in the first term on the right hand side of Eq. (1). Thus, the divergence D does *not* affect $\hat{\Lambda}$ directly, but D affects the alignment indirectly via its presence in the vorticity equation. In turbulent nonbuoyant flames, the density reduction causes D to be positive and thus creates a sink of vorticity[5,11] in the reaction zone. Accordingly, a region of weak vorticity and strong strain is created in the reaction zone of turbulent nonbuoyant flames.[6] The implication of this result in turbulent buoyant flames will be discussed in Sec. III.

The present work aims at addressing the following two points: *First*, as numerous studies of the vorticity-strain alignment indicate certain universality, we would like to investigate whether our results for buoyant flames show the same trends, and to understand why these universality trends (or lack of) exist.

Second, we would like to study the alignment of the scalar gradient vector ∇F with the strain eigenvectors, and establish whether this ∇F alignment is conditional on the

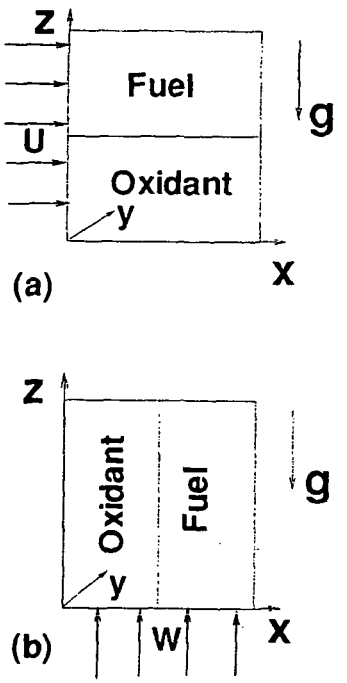

FIG. 1. Initial configuration. Cross-section of the solution domain. (a) Horizontal flame. (b) Vertical flame. U and W (see the arrows) denote the direction of the mean flow in x and z directions, respectively.

value of the mixture fraction F. The alignment of ∇F with the strain eigendirections has direct relevance to the chemical reaction process in turbulent nonpremixed flames since it controls the temporal development of the scalar dissipation rate and subsequently the progress of the chemical reaction.

The motivation for studying the alignment of strain, vorticity and scalar gradient in a buoyant nonpremixed flame is the unique feature of this flow of consisting of regions of quite distinct alignment characteristics as will be discussed later.

The paper is organized as follows: We present a brief description of the flow, and the solution method of the governing equations in Sec. II. We discuss the vorticity-strain alignment characteristics in Sec. III. We introduce a quantity, Ψ, to measure the relative magnitude of vorticity with respect to strain in Sec. III A. We examine the regions in the flow field having different Ψ characteristics in Sec. III B. We examine the vorticity-strain alignment pdf's in these in Sec. III C. In Sec. III D, we study the effects of the vorticity-strain alignment characteristics on the scalar gradient-strain alignment by examining the evolution equation of the scalar gradient vector [Eq. (4)]. We discuss the universality of the alignment results in Sec. IV.

II. FLOW DESCRIPTION

The two flow configurations (horizontal and vertical flames) chosen for the study are shown in Fig. 1. This figure shows a cross-section of the three-dimensional solution domain. The first configuration describes a horizontal flame for which the initial interface between the parallel and uniform mean-velocity streams of fuel and oxidant is perpendicular to the gravity vector. The second configuration describes a vertical flame for which the initial interface between the fuel and oxidant streams is parallel to the gravity vector. For both cases, the gravity vector is in negative z direction.

The flow is subsonic and the domain is unbounded and thus the thermodynamic pressure is assumed uniform in space and constant in time. In small Mach number turbulent flows with density variations arising from chemical energy release, the kinetic energy is small in comparison to the thermal energy. In order to compute such a flow, the full set of compressible equations may be employed. However, this has the computational disadvantage of a rather severe time step limitation in order to resolve the high frequency acoustic waves. In subsonic (small Mach number) flows, the time scale of the acoustic waves is much smaller than those associated with the convection processes. Since the acoustic fluctuations do not interact effectively with the fluid dynamics, they can be neglected. Simplifications to the fully compressible equations can therefore be made based on the small Mach number conditions. The resulting governing equations are similar to those of McMurtry *et al.*,[7] except that the buoyancy forces are included in our equations. The three-dimensional, time dependent, variable density continuity, Navier-Stokes and energy equations are solved together with the conservation equations of the mass fractions of the fuel and oxidizer. The chemical reaction between the fuel and oxidizer follows a single-step, irreversible, binary reaction with Arrhenius kinetics. The molecular viscosity, mass diffusion coefficient, thermal conductivity, and the constant-pressure specific heat are assumed to be invariant in time and space. The boundary conditions are periodic for the xz and yz plane boundaries, while a convective outflow boundary condition is imposed along the xy plane boundaries. The flow field is initialized with a prescribed energy spectrum which is proportional to ke^{-k} where k is the magnitude of the wave number vector.

The governing equations are discretized using a staggered grid and a semi-implicit second-order finite differencing scheme. The source terms in the energy and species equations are discretized using the Crank-Nicolson implicit method. The Poisson equation for the pressure is solved using a FFT combined with a tri-diagonal matrix solver following the algorithm by Schmidt *et al.*[8]

Three different grids with 96^3, 128^3 and $192\times96\times96$ points were used for the simulations with an initial Reynolds number based on Taylor microscale, $R_\lambda = 25$. Two grids with 128^3 and $192\times96\times96$ points were used with an initial $R_\lambda = 35$. In all the simulations, the resolution criteria $\eta k_{max} > 1.8$ is satisfied, where η is the Kolmogorov length scale and k_{max} is the maximum resolved wave number in the field.

The value of R_λ, and the number of grid points were prescribed such that the motion at the smallest scales are well resolved. This insures that the velocity and scalar gradients (including pressure gradients) are well resolved. The resolution accuracy is evaluated by comparing the results of the simulations using grids with successive refinement. For the nonbuoyant flame, the difference between the values of the pressure Hessian [Eq. (8)] obtained from the simulations with the two grids: 96^3 and 128^3, i.e., increasing the resolution by a factor of 2.37, resulted in less than 2% change in

the values of the pressure Hessian. For the buoyant flame, the gradients are steeper than those in the nonbuoyant flame. In order to resolve these gradients, we placed more points in the direction which has the steepest gradients, namely, the gravity direction. Here again, the values of the pressure Hessian from simulations with the two grids: 96^3 and 192×96^2 differed by less than 5% near the F_{st} surface.

The turbulence is allowed to develop without chemical reaction until the velocity derivative skewness reaches a value of approximately equal to 0.5. At that time, the chemical reaction is allowed to take place between the two nonpremixed streams of fuel and oxidizer.

The ranges of dimensionless numbers tested are: Damköhler number=1000, 5000, ∞; Froude number=7, 10, 18 and ∞; and $R_\lambda = 25$ and 35. This paper will present results of only two buoyant flames, one horizontal and the other vertical with Damköhler number=5000, and Froude number =10. The initial R_λ of the horizontal and vertical flames equals 25 and 35, respectively. We will refer also to the corresponding nonbuoyant flows of the two cases whenever necessary.

All the simulations continued until a non-dimensional time $t=6$, which equals about three eddy turnover times. The simulations are terminated before the expanding flow approaches the boundaries and starts to invalidate the imposed boundary conditions.

All the presented results are obtained at $t=5$ to insure that the maximum values of scalar dissipation, reaction rate, and temperature are already attained.

III. RESULTS

A. Strain-enstrophy state

The studies of Batchelor and Townsend,[1] Dresselhaus and Tabor,[4] and Boratav *et al.*[6] show that the relative magnitudes of the strain and rotation terms determine the vorticity/strain alignment characteristics. The rotation terms [see Eq. (5.4) of Batchelor and Townsend,[1] Eqs. (12) and (19) of Dresselhaus and Tabor,[4] Eq. (2) of Boratav *et al.*[6] or Eq. (1) in the present paper] consist of the vorticity, the rotation of the strain axes, and for the variable density case, the baroclinic vorticity production. For both incompressible[4] and compressible[6] flows, when the strain is dominant over the rotation, the material lines and the vorticity lines align along the direction of the maximum strain α. In this section, we focus on the relative magnitudes of the strain and vorticity. The effects of the rotation of the strain coordinates on the alignment will be briefly discussed in Sec. III C.

We examine the relative magnitudes of the strain and vorticity at each mesh point in a zone of containing the flame surface using a "*Strain-Enstrophy State*" plane. The abscissa and ordinate in that plane are the local enstrophy $\omega \cdot \omega/2 \equiv R_{ij}R_{ij}$ and the mean square strain rate $S_{ij}S_{ij}$. The polar coordinates of a given point on that plane are the distance, Δ, from that point to the origin and the counterclockwise angle, denoted by the *Strain-Enstrophy angle*, Ψ, and measured from the abscissa:[9]

$$\Delta = \sqrt{(S_{ij}S_{ij})^2 + (R_{ij}R_{ij})^2}, \tag{2}$$

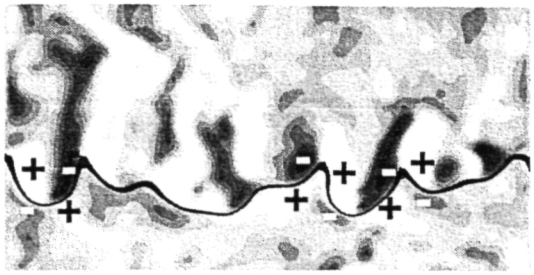

FIG. 2. Contours of out-of-plane vorticity on a xz plane at the mid-y location, for the horizontal flame, $t=5$, $Fr=10$, $Da=5000$. Only part of the solution plane is shown in the z (vertical) direction. Black and white correspond to negative and positive vorticity. The thick black curves correspond to a superposition of surfaces where $F \approx F_{st}$.

$$\Psi = \tan^{-1} \frac{S_{ij}S_{ij}}{R_{ij}R_{ij}}. \tag{3}$$

The definition of Ψ in (3) indicates that large values of Ψ ($\gg 45°$) are associated with strain-dominated regions, and smaller values of Ψ ($\ll 45°$) denote enstrophy-dominated regions. Since we are interested in the effects of chemical reaction (density variation) on the turbulence structure, we will focus our attention on a mixture fraction zone ($0.15 \leqslant F \leqslant 0.85$) surrounding the stoichiometric reaction surface ($F=0.5$).

In order to identify regions with different Ψ characteristics, we first examine the enstrophy characteristics of the different regions (Sec. III B) and then compute the Ψ characteristics (Sec. III C).

B. $R_{ij}R_{ij}$ characteristics

In order to determine the enstrophy ($R_{ij}R_{ij}$) characteristics of the different regions, we examine the vorticity isosurfaces, and investigate the importance of different terms in the enstrophy equation in these regions.

We present in Fig. 2 and Fig. 3 the out-of-plane vorticity contours for the horizontal and vertical flames, respectively. Positive and negative signs are marked to show the counter-

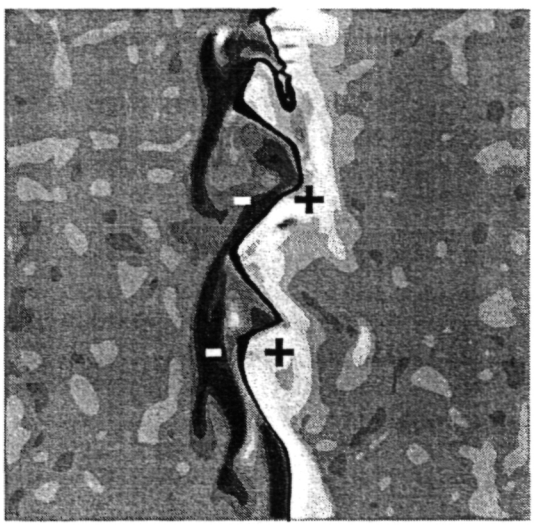

FIG. 3. Same as the previous figure, vertical flame.

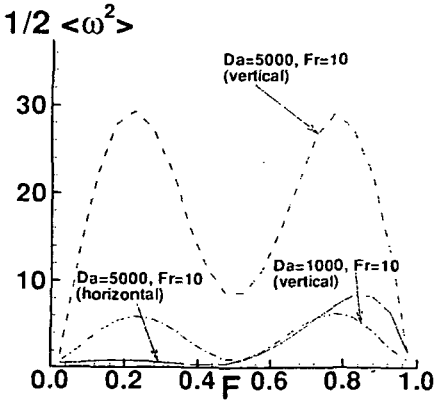

FIG. 4. F-band-averaged enstrophy $\omega\cdot\omega/2$. Curves correspond to: (a),(b) $Da=5000$, $Fr=10$ vertical (dashed) and horizontal (solid) flames. (c) $Da=1000$, $Fr=10$ vertical (dashed-dotted).

rotating vortices. The solid lines are the F-isosurfaces surrounding the F_{st} surface. It is seen from the figures that the horizontal flame F_{st} surface is saddled by *quadruples* whereas the vertical by *dipoles*. For the horizontal flame, the vorticity above the F_{st} surface is stronger than that below. For the vertical flame, the magnitudes of vorticity on both sides of the F_{st} surface are nearly the same.

Boratav *et al.*[6] show that the baroclinic torque is the main source of vorticity production in buoyant nonpremixed flames. This term changes sign across the F_{st} surface and vanishes at that surface because the density gradient changes signs across the reaction zone. They[6] also show that the largest magnitude of fluid velocity is along the gravity direction (w, the z-component of the velocity) and occurs at the F_{st} surface (i.e., at the location of minimum density). Away from the F_{st} surface, the fluid density increases, resulting in smaller w. Thus, $\partial w/\partial z$, which is the major contributor to $\nabla\cdot\mathbf{u}$ changes sign across the F_{st} surface. For regions of $F<F_{st}$, it is positive, and for $F>F_{st}$, it is negative, thus resulting in stronger vorticity in the former than in the latter, in the horizontal buoyant flame.

Similar arguments can be made about the vortex stretching term, namely, the dominant contributor to the stretching term is $\partial w/\partial z$, which changes sign across F_{st}. Thus the vorticity production due to the stretching is mainly in the regions of $F>F_{st}$, resulting in stronger vorticity there.

In summary, the strong baroclinic torque creates vorticity in both regions of $F>F_{st}$ and $F<F_{st}$. The velocity divergence and the vortex stretching terms produce stronger vorticity in regions of $F>F_{st}$ compared to that in $F<F_{st}$ in the horizontal flame. There is no such distinction between these regions in the vertical flame. The vorticity attains its minimum value at the F_{st} surface, as presented in Fig. 4, which shows the F-averaged enstrophy for different values of Froude and Damköhler numbers.

C. Ψ and alignment

Based on our analysis in the previous section, we classify the flow field into three distinct regions corresponding to the following mixture fraction values: (i) $F=F_{st}$; (ii) $F>F_{st}$; (iii) $F<F_{st}$. In order to have sufficiently large

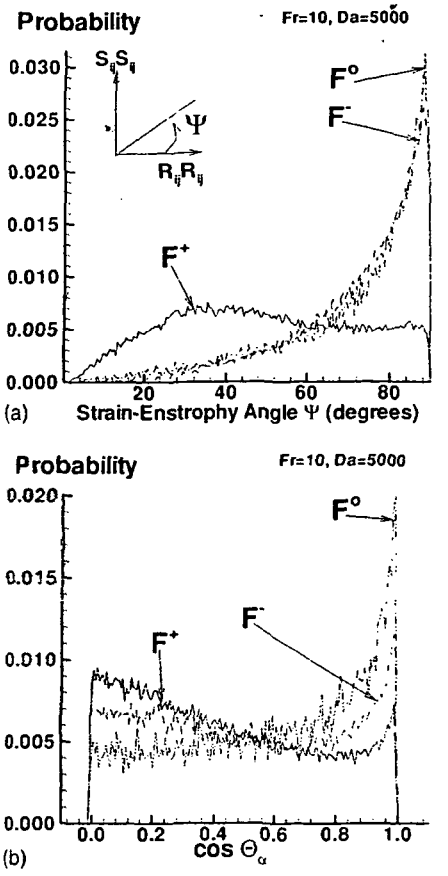

FIG. 5. Horizontal flame, $t=5$, $Fr=10$, $Da=5000$. Top: (a) pdf's of the strain-enstrophy angle Ψ for three F-bands: Solid: F^+, dashed: F^- and dashed-dotted: F^0. Bottom: (b) pdf's of the angle between vorticity and the eigenvector corresponding to the largest strain α of the rate of strain tensor. Same F-bands as above.

sample size for the statistics, we choose the following three F bands to compute the pdf of Ψ: (i) $0.45\leqslant F\leqslant 0.55$, denoted as the F^0 band; (ii) $0.50<F\leqslant 0.85$, denoted as the F^+ band; and (iii) $0.15\leqslant F<0.50$, denoted as the F^- band.

As discussed earlier, in the horizontal buoyant flame, the vorticity is small in F^0, and large in F^+. Also, the vorticity in F^+ is larger than that in F^-. Figure 5(a) shows that the flow is strain-dominated not only in F^0, which is expected, but also in F^- which is a manifestation of the fact that vorticity is small relative to the strain in these regions. On the other hand, as seen from Fig. 5(a), for F^+, the vorticity strength relative to strain increases.

Figure 5(b) presents the alignment characteristics for the same flow of Fig. 5(a). In this figure, the x axis is the cosine of the angle between the vorticity and the largest strain direction, denoted by $\cos\theta_\alpha$. The two strain-dominated bands, F^0 and F^- show α alignment trends, the former being stronger (i.e., larger probability values). On the other hand, the F^+ band in which the vorticity is more dominant than the strain, does *not* show α alignment trends but β (this is not shown here due to space limitation).

Figure 6(a) and (b) shows the results for the vertical flame, which are very similar to those for the horizontal flame, except that the statistics for F^- and F^+ are nearly identical, and thus only F^+ results are shown.

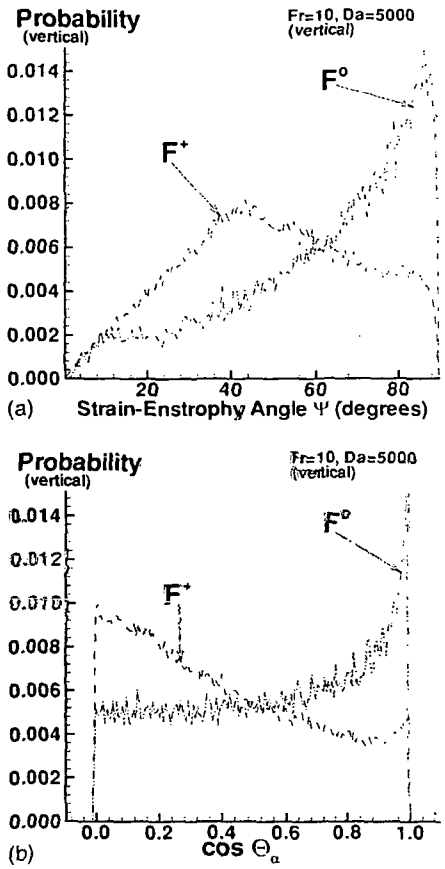

FIG. 6. Vertical flame, $t=5$, $Fr=10$, $Da=5000$. Top: (a) pdf's of the strain-enstrophy angle Ψ for two F-bands: Dashed: F^-, dashed-dotted: F^0. The other band F^- statistics are very close to those of F^- and therefore are *not* plotted. Bottom: (b) pdf's of the angle between vorticity and the eigenvector corresponding to the largest strain α of the rate of strain tensor. Same F-bands as above.

It should be mentioned that the strain rotation term Ω' is *not* included as part of the rotation terms in the definition of Ψ. Our computations show that this term is small compared to the other rotation terms (i.e., vorticity and baroclinic term), and thus it is not included in the Ψ definition.

D. Scalar gradient alignment

Now we discuss how the vorticity alignment influences the scalar gradient alignment with the strain eigenvectors. We consider the evolution equation for the scalar gradient:[10]

$$\frac{D}{Dt}(\nabla F) = -\mathbf{S}\cdot\nabla F + \frac{1}{2}\,\boldsymbol{\omega}\times\nabla F + \mathscr{V}_{\mathscr{F}}, \tag{4}$$

where $\mathscr{V}_{\mathscr{F}}$ denotes the viscous term. The contribution of the second term on the right hand side of Eq. (4) is to move ∇F toward a direction perpendicular to the vorticity vector. And as discussed in the previous section, the flow in the F^0 band is strain-dominated and the vorticity aligns with the α eigenvector. Thus, for the F^0 band, ∇F will move toward a plane containing $\mathbf{e}_\beta$ and $\mathbf{e}_\gamma$. In other words, ∇F will be strained *only* by β and γ strains. Since $|\gamma|>|\beta|$, the deformation of ∇F will be mostly along the γ direction. In incompressible turbulence, simulations by Kerr[2] and Ashurst *et al.*[3] show that the $|\gamma|/|\beta|$ ratio is about 4. Our simulations show that the

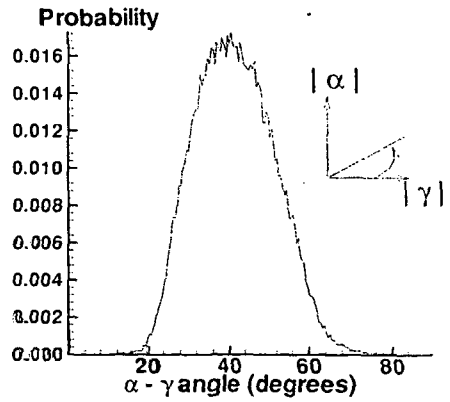

FIG. 7. Vertical flame, $t=5$, $Fr=10$, $Da=5000$. The pdf of the angle $\theta_{\alpha\text{-}\gamma}$ (see the text for definition). Note that the most likely value is approximately equal to 40°.

average of this ratio in the F^0 band is much larger than 4. Thus, ∇F is expected to align strongly along $\mathbf{e}_\gamma$ in the F^0 band.

On the other hand, for the F^+ (and F^- for the vertical flame) band(s), the vorticity aligns along the β eigenvector. Thus, ∇F will be on a plane strained only by α and γ strains. The dominant direction of deformation will depend on the relative magnitudes of α and γ. We quantify this relative magnitude by computing the α-γ angle $\theta_{\alpha\text{-}\gamma}$ defined as: $\theta_{\alpha\text{-}\gamma}=\tan^{-1}|\alpha|/|\gamma|$. Figure 7 displays the pdf of this angle for the vertical flame. The pdf shows that the most likely angle value is around 40°. This is equivalent to a ratio of $|\gamma|/|\alpha| = 1.19$.

The pdf of the cosine of the angle between ∇F and $\mathbf{e}_\gamma$ for the vertical buoyant flame is shown in Fig. 8. As discussed above, in the F^0 band, the $|\gamma|/|\beta|$ ratio is large, resulting in good alignment between ∇F and $\mathbf{e}_\gamma$ as seen in Fig. 8. On the other hand, in F^+ (and F^- for the vertical flame) band(s), as seen in Fig. 7, the pdf of the α-γ angle has its most likely value at an angle of 40° (note that cos 40°=0.77) which is consistent with the cosine of the angle between ∇F and γ eigendirection given in Fig. 8 in the F^+ band.

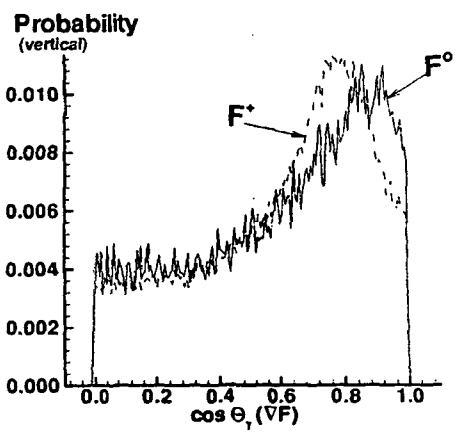

FIG. 8. Vertical flame, $t=5$, $Fr=10$, $Da=5000$. pdf's of the angle between ∇F and the eigenvector corresponding to the largest compressive (negative) strain γ of the rate of strain tensor. F-bands are: Solid: F^0. Dashed: F^+.

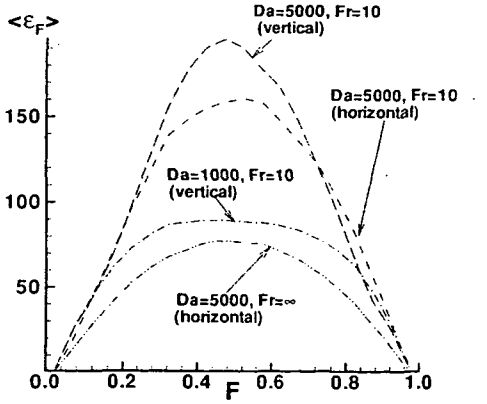

FIG. 9. F-band-averaged scalar dissipation ϵ_F for four different runs with $Da=1000$ and 5000, and $Fr=\infty$ and 10.

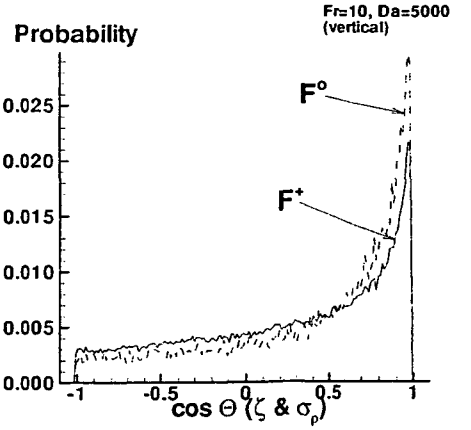

FIG. 10. The angle between the variable-density vortex stretching $\sigma_\rho \equiv \boldsymbol{\omega}/\rho \cdot \nabla \mathbf{u}$ and vorticity $\boldsymbol{\zeta} \equiv \boldsymbol{\omega}/\rho$. Only the vertical flame results are shown for two different F-bands for brevity.

In summary, our results show that both in the absence and presence of buoyancy, the F^0 band in nonpremixed flames is strain-dominated, mainly due to the small vorticity and large strain in this region. Accordingly, the vorticity (albeit small) aligns along the α direction in F^0. Consequently, the scalar gradient ∇F aligns along γ in F^0. Figure 9 shows that for a wide range of simulation parameters (not all are shown here), the peak scalar dissipation $\epsilon_F = \nabla F \cdot \nabla F$ always occurs within F^0.

IV. UNIVERSALITY OF ALIGNMENT

We have discussed in the previous sections that if the relative magnitudes of strain and vorticity are known, the preferential alignment directions of the vorticity and the scalar gradient vectors can be predicted. However, we did *not* explain why the dynamics moves toward such a state.

Recently, Gibbon and Heritage[12] and Galanti *et al.*[13] suggested that the alignment trends similar to those obtained here and in literature[2,3] can be a manifestation of an attracting fixed point of the Navier-Stokes equations and in this sense the alignment is universal. In this section, we compute certain quantities which appear in their[12,13] analysis and check whether our results are consistent with the existence of such an attracting solution.

Gibbon and Heritage[12] and Galanti *et al.*[13] indicated that the fixed point in the Navier-Stokes equations is associated with the angle θ between the vorticity and vorticity-stretching vector. This angle is given by:[12,13]

$$\theta = \tan^{-1} \frac{|\boldsymbol{\omega} \times \mathbf{S} \cdot \boldsymbol{\omega}|}{\boldsymbol{\omega} \cdot \mathbf{S} \cdot \boldsymbol{\omega}}. \tag{5}$$

When $\theta=0$, the vorticity and stretching vectors are parallel and the vorticity is stretched. Also, when the vorticity aligns with an eigenvector of the rate of strain tensor, then the vortex stretching vector $\mathbf{S} \cdot \boldsymbol{\omega}$ will also align with the vorticity, resulting in $\theta=0$ or $\theta=\pi$. For Burgers vortex, θ value is strictly equal to zero. It is shown[12,13] that cos θ approaches unity as the solutions move to the attracting fixed point.

The above analysis can be extended to the variable density case[12] if $\boldsymbol{\zeta} \equiv \boldsymbol{\omega}/\rho$ is used instead of the vorticity $\boldsymbol{\omega}$, and the variable density stretching, $\sigma_\rho \equiv (\boldsymbol{\omega}/\rho) \cdot \nabla \mathbf{u}$ is used instead of $\mathbf{S} \cdot \boldsymbol{\omega}$. Figure 10 shows the pdf of the angle between σ_ρ and $\boldsymbol{\zeta}$ in the vertical flame for the F^0 and F^+ bands; the horizontal flame results in these bands are similar. As expected, since the vorticity aligns with α in F^0 and with β in F^+, the cos θ pdf's have their most-likely values close to unity.

A quantity whose evolution has been examined in detail[12,13] is the scalar Λ_S (in Ref. 13, α) defined as:

$$\Lambda_S \equiv \frac{\boldsymbol{\omega} \cdot \mathbf{S} \cdot \boldsymbol{\omega}}{\boldsymbol{\omega} \cdot \boldsymbol{\omega}}, \tag{6}$$

for incompressible flows. For the Burgers vortex, Λ_S is equal to the applied external strain which is positive. For the attracting solution given in Refs. 12 and 13, the solution has a stable fixed point for $\Lambda_S > 0$. For the variable density flows, this quantity is defined as:

$$\Lambda_S \equiv \frac{(\boldsymbol{\omega}/\rho) \cdot \mathbf{S} \cdot (\boldsymbol{\omega}/\rho)}{(\boldsymbol{\omega}/\rho) \cdot (\boldsymbol{\omega}/\rho)}. \tag{7}$$

The F-averaged Λ_S distributions for the horizontal and vertical flames are shown in Fig. 11. We note that Λ_S values are positive in all F bands. Also, the largest Λ_S values on the average are in the F^0 band for both the vertical and horizontal flames, due to the fact that the denominator, $(\boldsymbol{\omega}/\rho) \cdot (\boldsymbol{\omega}/\rho)$ in (7) is small compared to the numerator, in that band.

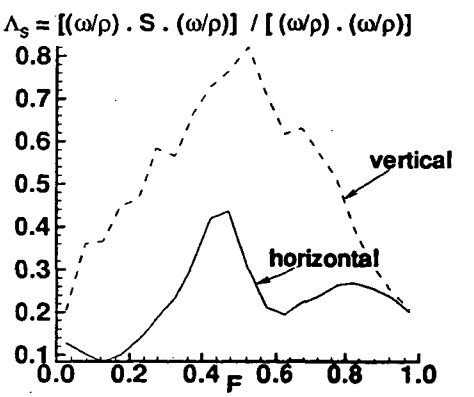

FIG. 11. F-averaged Λ_S values for the horizontal and vertical flames.

Another scalar quantity of interest[12,13] is Λ_P, which is related to the pressure Hessian **P**. For the variable density flows, the pressure Hessian **P** and Λ_P are given by:[12,13]

$$\mathbf{P} \equiv P_{\rho,ij} \equiv \frac{\partial}{\partial x_i}\left(\rho^{-1}\frac{\partial P}{\partial x_j}\right), \tag{8}$$

$$\Lambda_P \equiv \frac{(\omega/\rho)\cdot\mathbf{P}\cdot(\omega/\rho)}{(\omega/\rho)\cdot(\omega/\rho)}. \tag{9}$$

For Burgers vortex, the quantity Λ_P is strictly negative. For the attracting solution given by Refs. 12 and 13, as the solution moves towards the fixed point, Λ_P becomes negative.

Our simulations show that Λ_P is negative for all F bands for both the vertical and horizontal flames. Λ_P attains its peak negative (minimum) value in the F^0 band for both flames.

Finally, we examine how buoyancy changes the character of the pressure Hessian tensor **P**: Eq. (8) shows that for constant density, the pressure Hessian tensor $P_{\rho,ij}$, is a symmetric tensor and its eigenvalues are real. This is *not* the case for the variable density flow. As an example, we write the following two elements of $P_{\rho,ij}$:

$$P_{\rho,xz} = \frac{\partial}{\partial x}\left(\frac{1}{\rho}\right)\frac{\partial P}{\partial z} + \frac{1}{\rho}\frac{\partial^2 P}{\partial x \partial z},$$
$$P_{\rho,zx} = \frac{\partial}{\partial z}\left(\frac{1}{\rho}\right)\frac{\partial P}{\partial x} + \frac{1}{\rho}\frac{\partial^2 P}{\partial z \partial x}, \tag{10}$$

and the two elements are *not* necessarily equal in the presence of buoyancy. Therefore, buoyancy creates eigenvalues of $P_{\rho,ij}$ which are complex.

To verify this argument, we have computed the eigenvalues of $P_{\rho,ij}$ for both horizontal and vertical flames. The results of the two cases are similar and thus we present only those of the vertical flame. We use the notation introduced by Chong *et al.*[14] to classify the eigenvalues of $P_{\rho,ij}$. For the variable density case, the sum of the eigenvalues denoted by the invariant P is *not* necessarily zero, and thus the categories of $P>0$ and $P<0$ exist.

We find that, for the vertical flame, 85% of all mesh points belong to one of the eigencategories with all real eigenvalues. Following Chong *et al.*,[14] these categories with *only* real eigenvalues are labeled as $1a$ (all negative eigenvalues), $1b$ (all positive eigenvalues), $6a$ (two negative, one positive eigenvalue) and $6b$ (two positive and one negative eigenvalue). They contain, respectively, 6.6%, 7.2%, 35.72% and 34.9% of all the mesh points. The rest of the points (15%), are distributed among the categories $9a$, $9b$, $10a$ and $10b$ which have one complex conjugate and one real eigenvalue. (See Ref. 14 for details of the classification of eigenvalues.) They contain respectively 4.9%, 2.8%, 3.1% and 4.7% of all the points.

Figure 12 shows the pdf's of the strain-enstrophy angle Ψ for each of these eigencategories. In this figure, the lines for categories with real eigenvalues which contain more points appear smoother. As was discussed earlier, in the F^0 band, the Ψ values are close to 90°, and we see from Fig. 12 that they belong to either $1a$ (i.e., $---$) or $6a$ (i.e., $+--$).

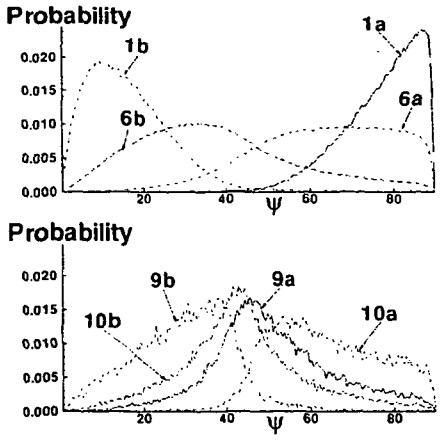

FIG. 12. Strain-enstrophy angle Ψ pdf's for different types of pressure Hessian eigenvalues. The labels of each group is taken from Chong *et al.* (1990). Top: Groups 1a, 1b, 6a and 6b with only real eigenvalues. Bottom: Groups 9a, 9b, 10a and 10b with one conjugate pair complex eigenvalue. Vertical flame.

Figure 12 also shows that at the other extreme of the Ψ pdf's (i.e., $\Psi \approx 0°$) where vorticity dominates over strain, most points belong to the category $1b$ (i.e., $+++$). Between the two extremes of Ψ (i.e., $\Psi \approx 0°$ and $\Psi \approx 90°$), all the categories with complex eigenvalues are seen (Fig. 12) in addition to the group $6b$ which has all real eigenvalues. Recall from Fig. 6(a) that mesh points with $\Psi \approx 40°$ belong to the F^+ and F^- bands.

We conclude that buoyancy produces complex $P_{\rho,ij}$ eigenvalues in the F^+ (and F^- for the vertical flame) band(s). On the other hand, the F^0 band (which has $\Psi \approx 90°$) has mostly real $P_{\rho,ij}$ eigenvalues indicating that buoyancy effects are *not* considerable at the flame surface.

V. CONCLUDING REMARKS

In turbulent nonpremixed flames, buoyancy effects can be summarized as follows: Buoyancy generates strong vortices on both sides of the flame surface (F_{st}), and thus reduces the strain-dominance in the field. This reduction results in the vorticity alignment with the β strain away from the flame surface.

The strain-enstrophy angle Ψ, can be used to determine the regions in which α or β alignment trends are expected. The motivation for introducing Ψ is based on the alignment equation [Eq. (1)] which we derived for the variable density case. This equation indicates that in regions where strain dominates over vorticity (or equivalently the baroclinic term), α alignment is expected.

The alignment characteristics of the region near F_{st} (denoted by F^0) are *not* affected by buoyancy. This result is of importance to the scalar field. The peak scalar gradient (dissipation rate ϵ_F) occurs in F^0 regardless of the presence of the buoyancy.

Our results are consistent with the recent analysis of Gibbon and Heritage[12] and Galanti *et al.*[13] which suggested that the Navier-Stokes equations evolve toward an attracting solution. All the requirements for the solution of the Navier-Stokes equations to move to an attracting fixed point are met

in the flows we considered in this paper. One drawback of the analysis of Refs. 12 and 13 is that it does *not* distinguish between the α alignment and the β alignment. Also, the analysis[12,13] ignores the dynamics of regions with large strain/small vorticity. In fact, along a vorticity null line Λ_S and Λ_P are undefined.

ACKNOWLEDGMENTS

This work is supported by NASA microgravity Grant No. NAG3-1601. The computations were performed on Cray C-90 at NASA Ames and at San Diego Supercomputing Center. This research was also supported in part by the University of California Irvine, through an allocation of computer resources.

[1]G. K. Batchelor and A. A. Townsend, "Turbuleat diffusion," in *Surveys in Mechanics* (Cambridge University Press, Cambridge, 1956).
[2]R. M. Kerr, "Histograms of helicity and strain in numerical turbulence," Phys. Rev. Lett. **59**, 783 (1987).
[3]Wm. T. Ashurst, A. R. Kerstein, R. M. Kerr, and C. H. Gibson, "Alignment of vorticity and scalar gradient with strain rate in simulated Navier-Stokes turbulence," Phys. Fluids A **30**, 2343 (1987).
[4]E. Dresselhaus and M. Tabor, "The kinematics of stretching of material elements in general flow fields," J. Fluid Mech. **236**, 415 (1992).
[5]K. K. Nomura and S. E. Elghobashi, "The structure of inhomogeneous turbulence in variable density nonpremixed flames," Theor. Comput. Fluid Dyn. **5**, 153 (1993).
[6]O. N. Boratav, S. E. Elghobashi, and R. Zhong, "On the alignment of the α-strain and vorticity in turbulent nonpremixed flames," Phys. Fluids **8**, 1 (1996).
[7]P. A. McMurtry, J. J. Riley, and R. W. Metcalfe, "Effects of heat release on the large-scale structure in turbulent mixing layers," J. Fluid Mech. **199**, 297 (1989).
[8]H. Schmidt, U. Schumann, and H. Volkert, "Three-dimensional, direct and vectorized eliptic solvers for various boundary conditions," Report DFVLR-Mitt 84-15 (1984).
[9]O. N. Boratav and R. B. Pelz, "Structures and structure functions in the inertial range of turbulence," Phys. Fluids **9**, 1400 (1997).
[10]K. K. Nomura, "Small-scale structure of turbulence in a nonpremixed reacting flow with and without energy release," Ph. D. Dissertation, University of California Irvine (1994).
[11]E. Meiburg, "Lagrangian simulation of diffusion flames," Combust. Sci. Technol. **71**, 1 (1990).
[12]J. D. Gibbon and M. Heritage, "Angular dependence and growth of vorticity in the three-dimensional Euler equations," Phys. Fluids **9**, 901 (1997).
[13]B. Galanti, J. D. Gibbon, and M. Heritage, "Vorticity alignment results for the 3D Euler and Navier-Stokes equations," Nonlinearity **10**, 1675 (1997).
[14]M. S. Chong, A. E. Perry, and B. J. Cantwell, "A general classification of three-dimensional flow fields," Phys. Fluids A **2**, 765 (1990).